Protective Effect of Buyang Huanwu Decoction on Neurovascular Unit in Alzheimer's Disease Cell Model via Inflammation and RAGE/LRP1 Pathway

Authors' Contribution:
Study Design A
Data Collection B
Statistical Analysis C
Data Interpretation D
Manuscript Preparation E
Literature Search F
Funds Collection G

AG 1 Bin Liu*
B 1 Guoliang Liu*
B 2 Yueyang Wang
D 1 Yuan Yao
B 1 Guanzhuo Wang
C 1 Xia Lei
A 1,3 Ning Zhang
D 1 Xiaohong Dong

1 Jiamusi College, Heilongjiang University of Chinese Medicine, Jiamusi, Heilongjiang, P.R. China
2 College of Acupuncture, Heilongjiang University of Chinese Medicine, Harbin, Heilongjiang, P.R. China
3 College of Pharmacy, Heilongjiang University of Chinese Medicine, Harbin, Heilongjiang, P.R. China

Background:
The aim of this study was to investigate the protective mechanism of neurovascular unit of Buyang Huanwu decoction (BYHWD) in an Alzheimer's disease (AD) cell model via RAGE/LRP1 pathway and find a reliable target for Alzheimer's disease treatment.

Material/Methods:
Rat brain microvessel endothelial cells (BMECs) were cultured in 10% FBS and 1% penicillin/streptomycin. The AD model was established by administration of 24 μmol/L amyloid-β peptides 25~35. Different concentrations of BYHWD (0.1 mg/mL, 1 mg/mL, and 10 mg/mL) were added as the drug intervention. The morphology of the cells was observed by light microscopy and the ultrastructure of the cells was observed by microscopy. The inflammatory factors IL-1β, IL-6, TNF-α, and Aβ_{25-35} were detected by ELISA. Flow cytometry was used to assess the apoptosis rate. The expressions of RAGE, LRP1, ICAM-1, VCAM-1, Apo J, Apo E, and NF-κBp65 were detected by Western blotting.

Results:
The structure of cells in BYHWDM and BYHWDH gradually recovered with increasing dose. BYHWD decreased the apoptotic rate of BMECs induced by Aβ_{25-35}. The cells treated with different concentrations of BYHWD had significant difference in terms of anti-apoptotic effect. The therapeutic effect of BYHWD on AD was via the RAGE/LRP1 and NF-κBp65 pathways.

Conclusions:
BYHWD regulates Aβ metabolism via the RAGE/LRP1 pathway, inhibits vascular endothelial inflammation induced by ICAM-1 and VCAM-1 via the NF-κBP65 pathway, and promotes morphological changes induced by Aβ-induced brain microvascular endothelial cell damage.

MeSH Keywords:
Alzheimer Disease • Endothelial Cells • Microvascular Decompression Surgery

Full-text PDF:
https://www.medscimonit.com/abstract/index/idArt/917020

📄 3271   🖽 1   📊 9   📚 29

Background

Alzheimer's disease (AD) is a chronic neurodegenerative disorder in multiple brain regions, characterized by the accumulation and deposit of plaques of amyloid-β (Aβ) peptide in the brain [1–3]. AD generally occurs in middle to late adulthood and is always associated with decreased cognitive capabilities. Based on clinical and population-based studies, approximately 200 000 people under 65 years of age have AD [4,5]. In the last 30 years, research has suggested that receptor for advanced glycation end-products (RAGE), which is a multi-ligand receptor located on the immunoglobulin superfamily of cell surface molecules, is involved in the pathogenesis of neurological dysfunction and death in people with AD [6,7]. A brief pulse of cellular activation can be converted to sustained cellular dysfunction and tissue destruction by engagement of RAGE [8,9]. Recently, a study suggested that abnormal translocation of Aβ across the blood-brain barrier plays a vital role on AD [10]. Translocation of Aβ across the blood-brain barrier is mainly realized through the RAGE and low-density lipoprotein receptor-related protein1 (LRP1). RAGE acts as a vital transporter in regulating influx Aβ, whereas the efflux of Aβ is achieved by LRP1 [11–14]. The increase of Aβ production is caused by various reasons; the decreased clearance rate leads to accumulation of Aβ in brain parenchyma, and the formation of senile plaque is the basic process of AD [15].

Buyang Huanwu decoction (BYHWD), a traditional Chinese medicine (TCM) prescription, plays a role in blood circulation. In animal experiments, BYHWD has been proven to protect nerves, promote angiogenesis, and improve functioning [1,16]. Furthermore, studies have demonstrated that BYHWD promotes the recovery of nerve function and angiogenesis by enhancing VEGFR2 phosphorylation through the PI3K/Akt signaling pathway [17,18], and improves denervation dependent muscle atrophy by increasing ANGPTL4 expression [19]. The aim of the present study was to define the protective mechanism of BYHWD in the neurovascular unit via RAGE/LRP1 pathway in an AD cell model and find a reliable target for AD treatment.

Material and Methods

Preparation

According to the original prescription from the "TCM Prescriptions Dictionary", BYHWD consists of 7 Chinese herbs (Table 1) [20]. All dried herbs were purchased from the First Affiliated Hospital of Heilongjiang University of Traditional Chinese Medicine by Professor Zhongguang Zhou. The decoction was prepared [3,17], and freeze-dried into dry powder by Professor Ning Tian at the Experimental Center of Heilongjiang University of Traditional Chinese Medicine. All herbal chemical ingredients of drugs were extracted referring to standard methods listed in the National Pharmacopoeia of China to maintain the consistency. The dry powder of BYHWD was dissolved in sterile water, and then was prepared into a saturated solution.

Establishment of AD cell model

The primary rat brain microvessel endothelial cells (BMECs) were purchased from Shanghai Asiqi Biological Engineering Company (China). The study was approved by the Ethics Committee of the First Affiliated Hospital of Heilongjiang University of Traditional Chinese Medicine. The BMECs was seeded into a culture flask and cultured with DMEM medium containing 10% fetal bovine serum (FBS) (Bovogen, Australia) and 1% penicillin/streptomycin (HyClone, USA) in a 37°C incubator with 5% CO_2 and 100% humidity. BMECs in logarithmic growth phase were adjusted to 1.0×10^5/mL cell suspension with culture medium. We seeded 5 mL of cell suspension into a 25-cm^2 culture flasks and cultured it for 24 h in an incubator with 5% CO_2 at 37°C. After cell adhesion was achieved, the primary culture medium was discarded and culture medium containing 24 μmol/L $Aβ_{25–35}$ (Bioss Biotechnology, Beijing, China) cells was added and incubated for 24 h to create the AD cell model.

Drug administration

The BMECs were seeded into 6 flasks randomly divided into 6 groups: 1) Control group (Control), cells were cultured with

Table 1. Components of Buyang Huanwu decoction.

| Family	English name	Chinese name	Batch number	Weight
Leguminosae	Astragalus mongholicus	Huang qi	131109	120 g
Umbelliferae	Angelica root	Dang gui	131001	6 g
Ranunculaceae	Red peony root	Chi shao	121003	4.5 g
Umbelliferae	Sichuan lovage rhizome	Chuan xiong	20140501	3 g
Megascolecidae	Earthworm	Di long	121002	3 g
Rosaceae	Peach seed	Tao ren	20140401	3 g
Feverfew	Carthamus tinctorius	Hong hua	130901	3 g
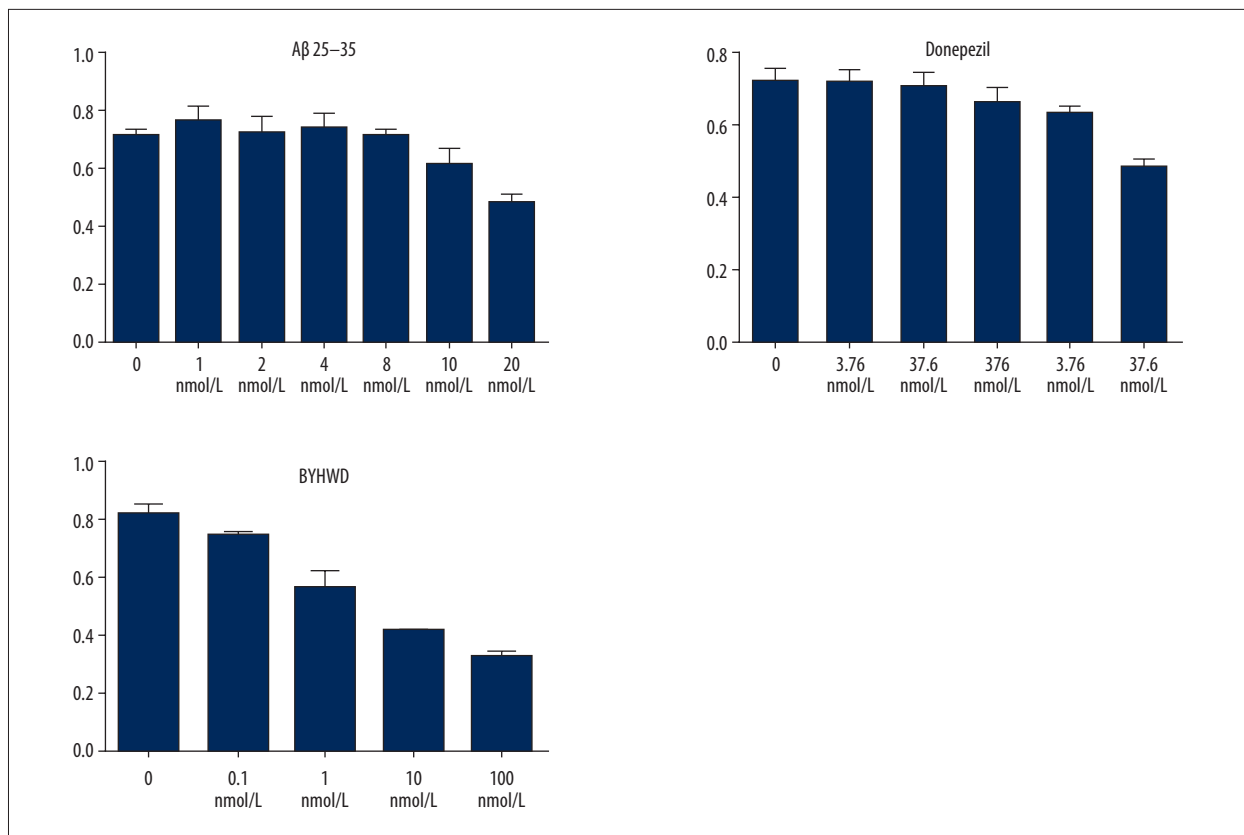
Figure 1. Effect of Aβ$_{25-35}$, Donepezil, and BYHWD on cell proliferation rate at different concentrations.

drug-free medium (10% FBS, 1% penicillin/streptomycin); 2) Model group (Model), the cells were incubated with drug-free medium after the establishment of AD model; 3) Donepezil group (Positive control), the cells were incubated with 37.6 μM Donepezil (Beijing Braun Technology Co., Beijing, China) cell medium after establishment of the AD model; 4) Low-dose BYHWD group (BYHWDL), the cells were treated with 0.1 mg/mL BYHWD after establishment of the AD model; 5) Middle-dose BYHWD group (BYHWDM), the cells were treated with 1 mg/mL BYHWD after establishment of the AD model; and 6) High-dose BYHWD group (BYHWDH), the cells were treated with 10 mg/mL BYHWD after establishment of the AD model.

Proliferation assay

Cells density was adjusted to 5×10^3~1×10^4/mL, 100 μL/well, and then inoculated to 96-well culture plates (8 wells in each group) for 24 h. Then, 180 μL of different concentrations of BYHWD (0.1 mg/mL, 1 mg/mL, and 10 mg/mL) were added into each of the wells according to the grouping scheme. After 20 h of culturing, 20 ul of MTT solution (Sigma-Aldrich Chemical Company, St Louis, USA) at a concentration of 5 mg/ml was added into each of the wells, and the cells were incubated for an additional 4 h at 37°C. Next, 150 μL of DMSO (Solarbio, Beijing, China) was added into each of the wells and gently

shaken for 10 min to mix. The spectrophotometric absorbance was measured at a wavelength of 490 nm using a Multiskan MK3 microplate reader (Thermo Lab Systems, USA).

Microscopic observation

The treated BMECs were digested using 1 mL of 0.25% trypsin-EDTA (Bovogen, Australia) for 3 min and seeded into the 6-well culture plates after cell resuspension, and then cultured with drug for 24 h. Then, the cells were observed and photographed under an inverted microscope (Leica, Germany).

Giemsa staining

Cell density of the BMECs in the logarithmic growth phase was adjusted to 1.0×10^5/mL and seeded into 6-well culture plates. The culture medium of each of the wells was aspirated. The cells were then washed twice with PBS, fixed with 4% formaldehyde, stained with Giemsa solution (Solarbio, Beijing, China) for 20 min, and then destained with water. The plate was dried, observed, and photographed under a light microscope (Leica, Germany).
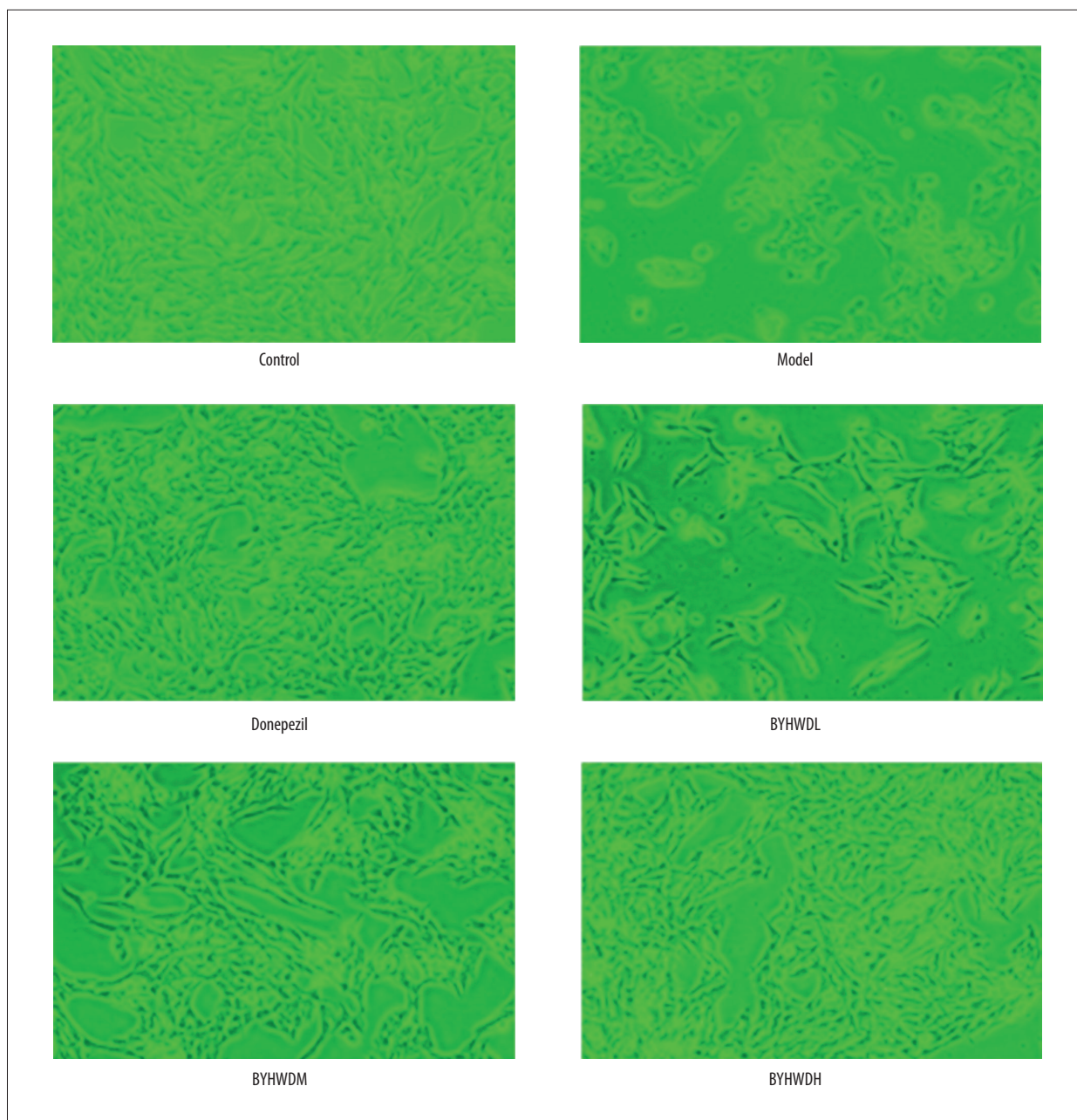
Figure 2. The morphology of BMECs as shown by microscopy (×100). Bar, 200 µm.

Electron microscopy

BMECs were digested with 0.25% trypsin for 3 min and centrifuged for 5 min at 2000 rpm. After washing 2 times with PBS, the cells were centrifuged again and the supernatant was discarded. The cells were then fixed with glutaraldehyde and 1% osmic acid, dehydrated with acetone, embedded in epoxy resin, and then cut into 60-nm ultrafine slices. After double staining with uranyl acetate and lead citrate, the slices were observed and photographed with a transmission electron microscope (Leica, Germany).

Apoptosis assay

Flow cytometry including annexin-V FITC (Beijing Baosai Biotechnology) and propidium iodide (PI) double staining were used to assess cell apoptosis. Briefly, after treatment, floating and trypsinized adherent cells were collected and washed with PBS 2 times. Then, the cells were resuspended with 100 µL PBS, after which 5 µL of FITC-marked annexin-V and 5 µl of PI were added, evenly mixed, and incubated in the dark for 15 min. Subsequently, 1×binding buffer was added to
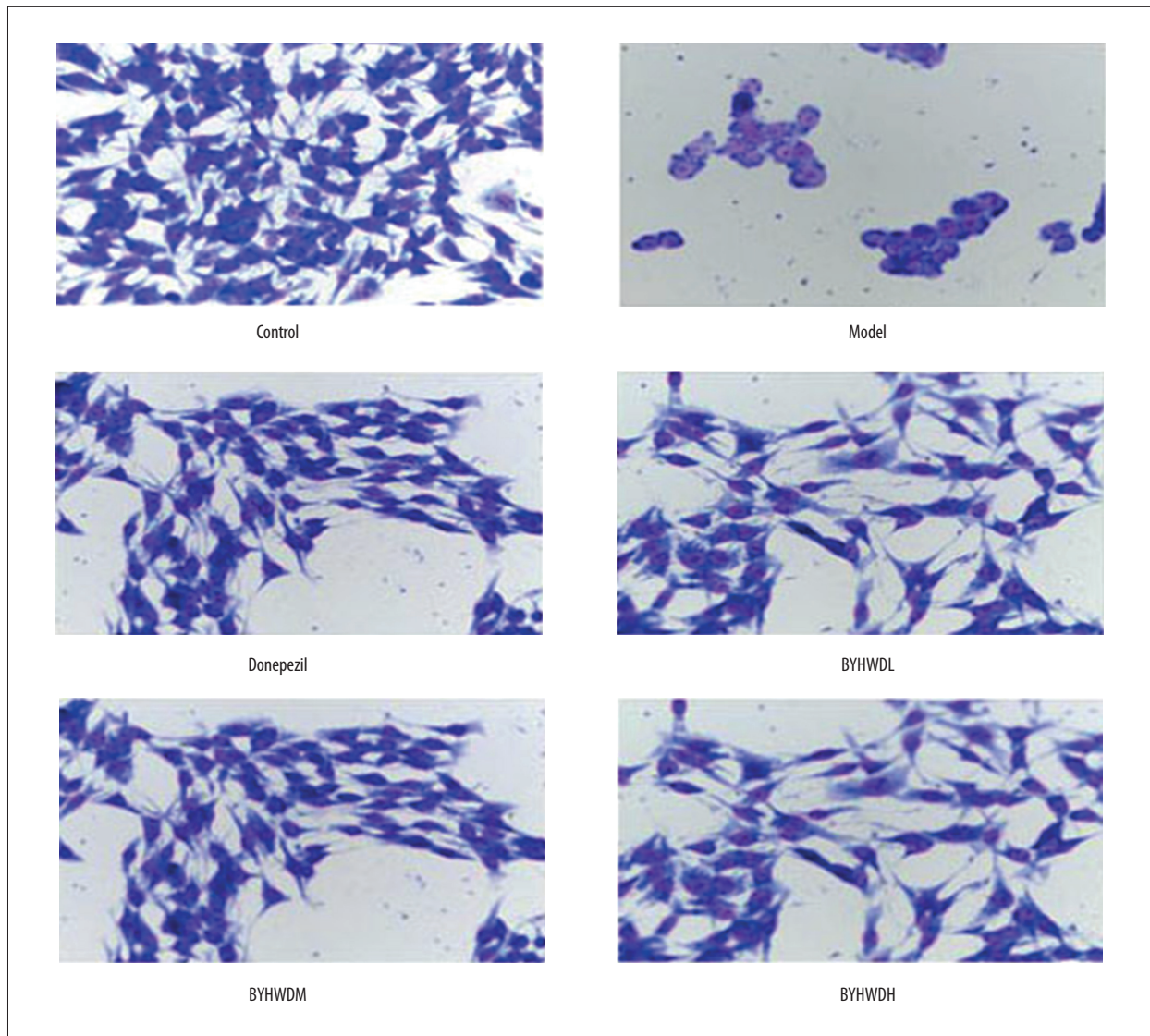
Figure 3. Giemsa staining to observe the morphology of BMECs.

each reaction tube. After 1 h, the cells were assessed by flow cytometry (Beckman; Palo Alto, CA, USA).

Enzyme-linked immunosorbent assay (ELISA)

The supernatant was collected and measured using ELISA kits (Xitang Company, Shanghai, China) according to the manufacturer's instructions. The test indicators included IL-1β, IL-6, TNF-α, and Aβ$_{25-35}$. Optical density was measured at 450 nm using a microplate reader (Thermo, USA).

Western blotting

The concentration of protein sample was detected by BCA Protein Assay Kit (Boster Biological Technology Co., Wuhan, China). The protein samples were mixed with 5×loading buffer,

and then boiled for 5 min. Equal amounts of protein (30 μg) were electrophoresed by 12% sodium dodecyl sulfate polyacrylamide gel electrophoresis. After electrophoresis, the targeted proteins on the gel were transferred onto a polyvinylidene difluoride (PVDF) membrane (Millipore Corp., Billerica, MA, USA) and blocked with 5% skim milk overnight at 4°C. After that, the membrane was incubated with primary antibodies at room temperature for 2 h. After 3 washes with TBST, the membrane was incubated with HRP-labelled secondary antibody for 1 h at room temperature. Subsequently, the PVDF was immersed into the electrochemiluminescence (ECL, USA) solution for 2 min in the dark. Finally, band intensity was quantified using Image J software (Rawak Software, Germany). The ratio of gray values between targeted band and the internal reference band was used as the relative expression of protein. The primary antibodies used in this study were: rabbit anti-RAGE
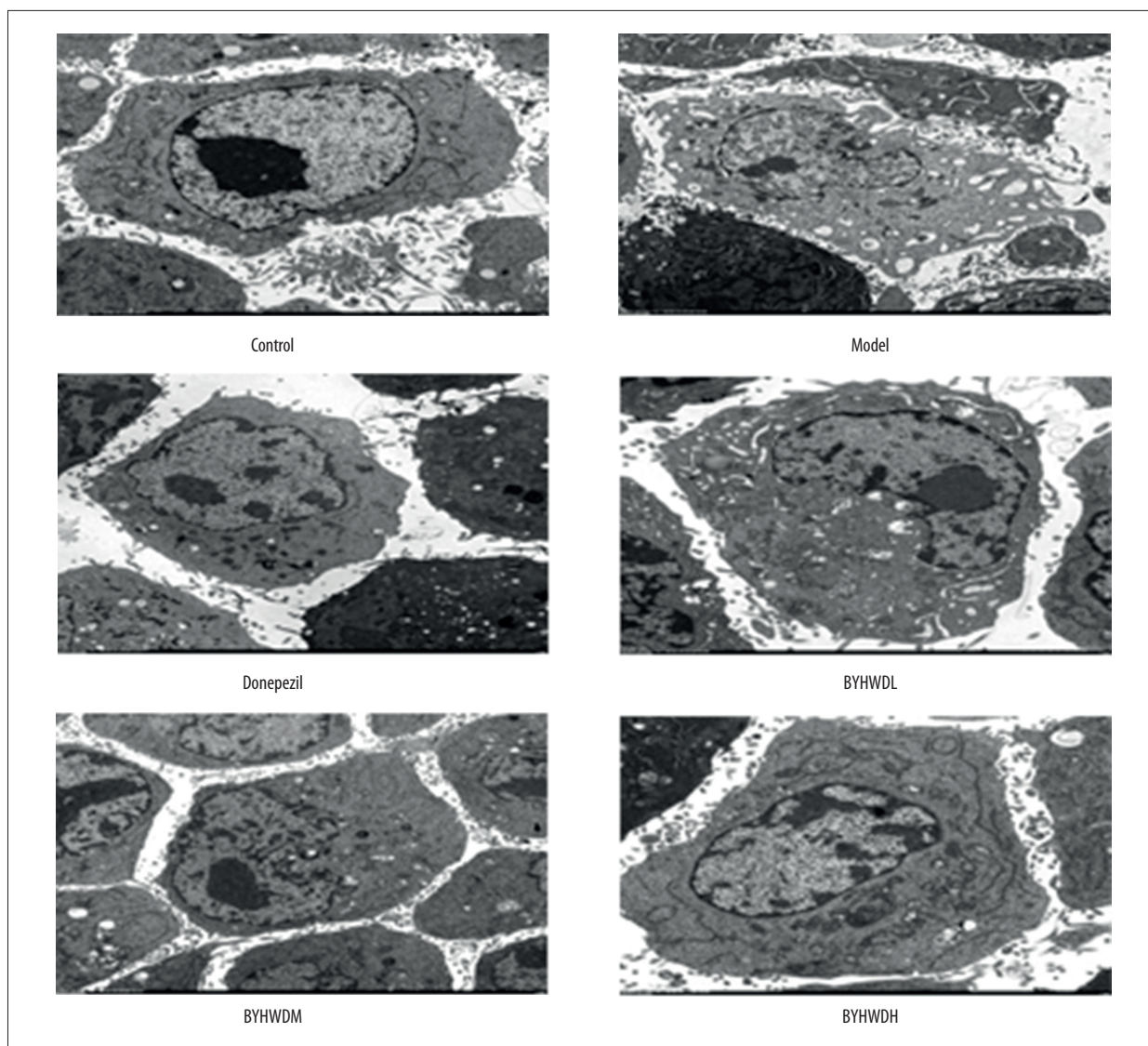
Figure 4. The ultrastructure of BMECs as shown by transmission electron microscopy (×1300).

antibody (CST, Danvers, MA, USA), rabbit anti-LRP1 antibody (CST, Danvers, MA, USA), rabbit anti-ICAM-1 antibody (CST, Danvers, MA, USA), rabbit anti-VCAM-1 antibody (CST, Danvers, MA, USA), rabbit anti-ApoJ antibody (CST, Danvers, MA, USA), rabbit anti-ApoE antibody (CST, Danvers, MA, USA), and rabbit anti-NFκB-p65 antibody (CST, Danvers, MA, USA), with β-actin (CST, Danvers, MA, USA) as the internal reference. The secondary antibodies used were: goat anti-rabbit HRP-conjugated IgG (Boster Biological Technology Co., Wuhan, China) and goat anti-mouse HRP-conjugated IgG (Boster Biological Technology Co., Wuhan, China). All secondary antibodies were diluted with WB Secondary Antibody Diluent (M3101, HaiGene, Shanghai, China). All experiments were repeated 3 times.

Statistical analysis

All data were analyzed by SPSS13.0 (SPSS, Inc., Chicago, IL, USA) software. All data were obtained from 3 independent experiments. All data are shown as means ± standard deviation (SD). Statistical significance of the data was determined using one-way analyses of variance (ANOVA) followed by a Student-Newman-Keuls (SNK) multiple comparison test. $P < 0.05$ was considered statistically significant.
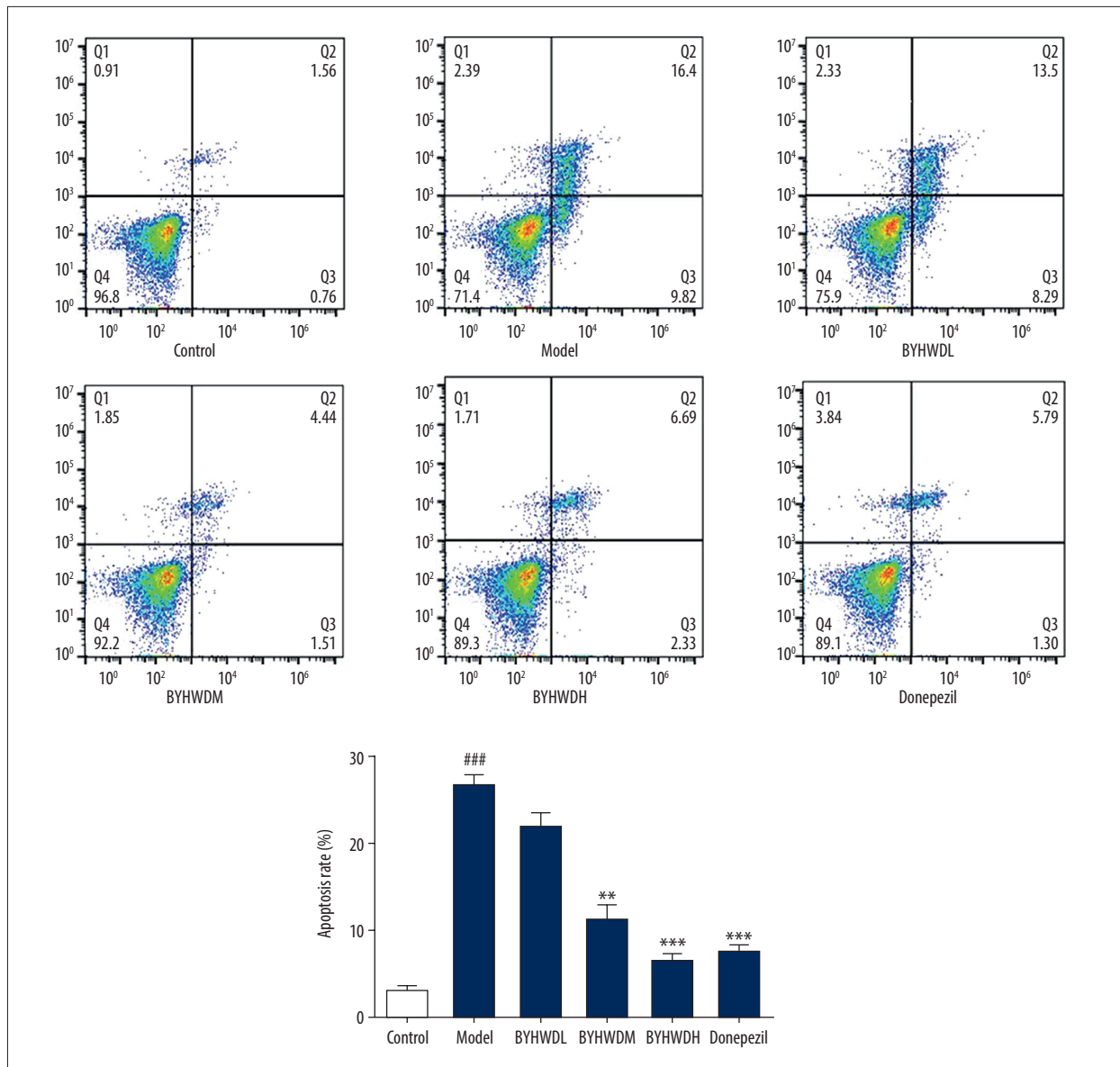
Figure 5. Effect of BYHWD on apoptosis at different concentrations. ### $P<0.001$, compared with control group; ** $P<0.01$, *** $P<0.001$, compared with model group.

Results

Effect of drugs on the proliferation of BMECs

MTT assays showed that the IC_{50} values of BYHWD, $A\beta_{25-35}$, and Donepezil were 1 mg/mL, 20 nmol/L, and 37.6 μmol/L, respectively. The experimental grouping was set up according to the value of IC_{50}. MTT assays showed that less than 10 nmol $A\beta_{25-35}$ inhibits the cell proliferation. The cell proliferation was obviously inhibited by 20 nmol $A\beta_{25-35}$, achieving half inhibition. The cell proliferation was obviously inhibited by 37.6 μmol/L Donepezil, while less than 37.6 μmol/L Donepezil had no obvious effect on cell proliferation. Less than 1 mg/mL BYHWD

had little or no effects on the inhibition of cell proliferation, but more than 1 mg/mL BYHWD had an obvious effect on cell proliferation, achieving half inhibition (Figure 1).

Microscopic observation of cell growth

In the control group, BMECs grew adherently and rapidly. The cells presented a rich cytoplasm and had fusiform or polygon shapes. In the model group, the cell proliferation was obviously slower and the cell adherence was weaker than in the control group, and the cell shape was changed from polygon to circle with the features of cells shrinkage and apparent loosening of cellular junctions. Compared with the Model
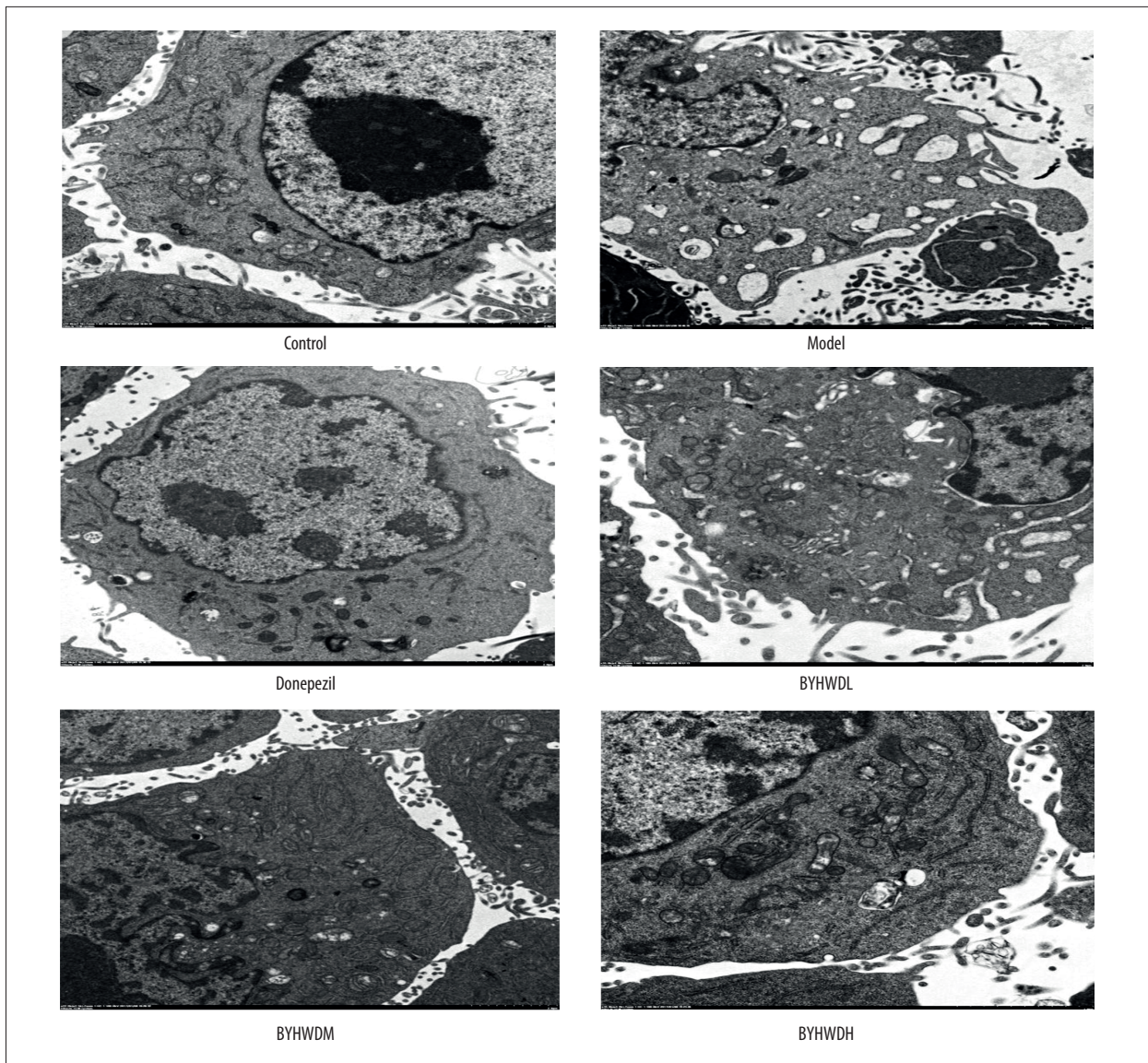
Figure 6. The apoptotic bodies of BMECs as shown by transmission electron microscopy (×22 000).

group, the cells in the Donepezil group had rapid growth and enhanced cell adhesion, the number of cells increased, and cell shape was restored (Figure 2). In the BYHWDL, BYHWDM, and BYHWDH groups, the cell adherence and growth rate increased gradually with increasing dose. In addition, the number of cells was gradually increased with increasing dose, and the shape of cells in the BYHWDH group was similar to that in the control group (Figure 2).

Giemsa staining

In the control group, the BMECs had fusiform or polygon shapes, and they were large and rich in cytoplasm. Multiple nucleoli were observed in the nucleus, and the cell membrane was intact. In the Model group, the shape of cells changed to round, the number of cells decreased, and the volume of cells was smaller. Moreover, the cells showed early apoptosis in the form of nucleus pyknosis and lysis, and chromatin margination. In contrast to the Model group, there were more cells in the Donepezil group, with less nucleus pyknosis and better cell morphology. In the BYHWDH, BYHWDM, and BYHWDL groups, there was more nucleus pyknosis, lysis gradually decreased, and the number of cells gradually increased with increasing dose. The morphology of cells in the BYHWDH group was similar to that of the Control group (Figure 3).

Electron microscopic observation of cell ultrastructure

In the Control group, the BMECs showed normal nucleus, rich cytoplasm, clear rough endoplasmic reticulum, and normal
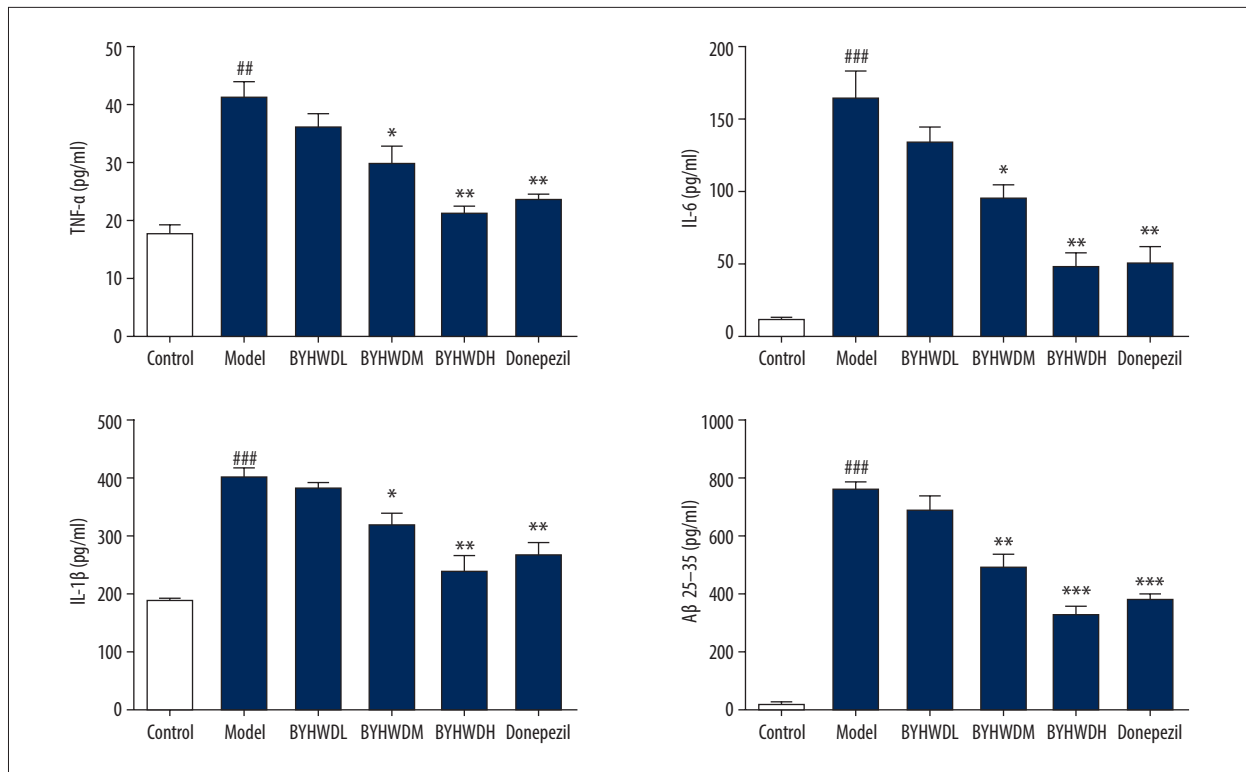
Figure 7. The inflammatory factor of IL-1β, IL-6, Aβ$_{25-35}$, and TNF-α detected by ELISA.

cytoplasm-to-nucleus ratios. In addition, microvilli and mitochondrial flocculent densities were observed. By contrast, cells in the Model group had nucleus pyknosis, abnormal nucleus-to-cytoplasm ratio, poor cytoplasm, expansion of rough endoplasmic reticulum, and widened perinuclear spaces. Additionally, vacuolar degeneration of mitochondria and limited microvilli were observed. Compared with the Model group, cells in the Donepezil group showed normal nucleus, rich cytoplasm, and clear rough endoplasmic reticulum and mitochondria. Moreover, there was microvilli and vacuolar degeneration in the cytoplasm. The structure of cells in the BYHWDL group was poor, while the structure of cells in the BYHWDM and BYHWDH groups gradually recovered with increasing dose (Figure 4).

Flow cytometry apoptosis detection

The protective effect of BYHWD on Aβ-induced BMECs was observed by Annexin-V-FITC/PI method. Compared with the Control group, flow cytometry analysis showed that there were significantly more BEMCs in the Model group (*P*<0.001). Compared with the Model group, the apoptotic rate of BMECs was significantly decreased in the BYHWDM and BYHWDH groups, especially in the BYHWDH group (*P*<0.01). The results indicated that BYHWD decreased the apoptotic rate of BMECs induced by Aβ (Figure 5).

Observation of apoptotic bodies by transmission electron microscopy (TEM)

In the Control group, the chromatin of apoptotic cells was condensated, condensed into small pieces, and gathered in a crescent or ring body around the nuclear membrane. The cytoplasm of apoptotic cells in the Control group was concentrated, the loose endoplasmic reticulum merged with the membrane to form many vacuoles, while mitochondria and the structure of endoplasmic reticulum did not change obviously. In the late stage of apoptosis, there were cell nucleus apoptotic bodies. The chromatin of necrotic cells was sparse and granular, with irregularly distributed and unclear boundaries. The cytoplasm was swollen, the organelle structure was damaged, and the cell membrane was incomplete. However, the cells treated with BYHWD showed significantly fewer apoptotic bodies. Furthermore, the cells treated with different concentrations of BYHWD had significantly different anti-apoptotic effects (Figure 6).

Inflammatory factors detected by ELISA

Compared with the Control group, the expression levels of IL-1β, IL-6, Aβ$_{25-35}$, and TNF-α in the Model group were significantly higher (P<0.01). In contrast to the Model group, the expression levels of IL-1β, IL-6, and TNF-α were significantly lower in the BYHWDM group (P<0.01). In the BYHWDH group,
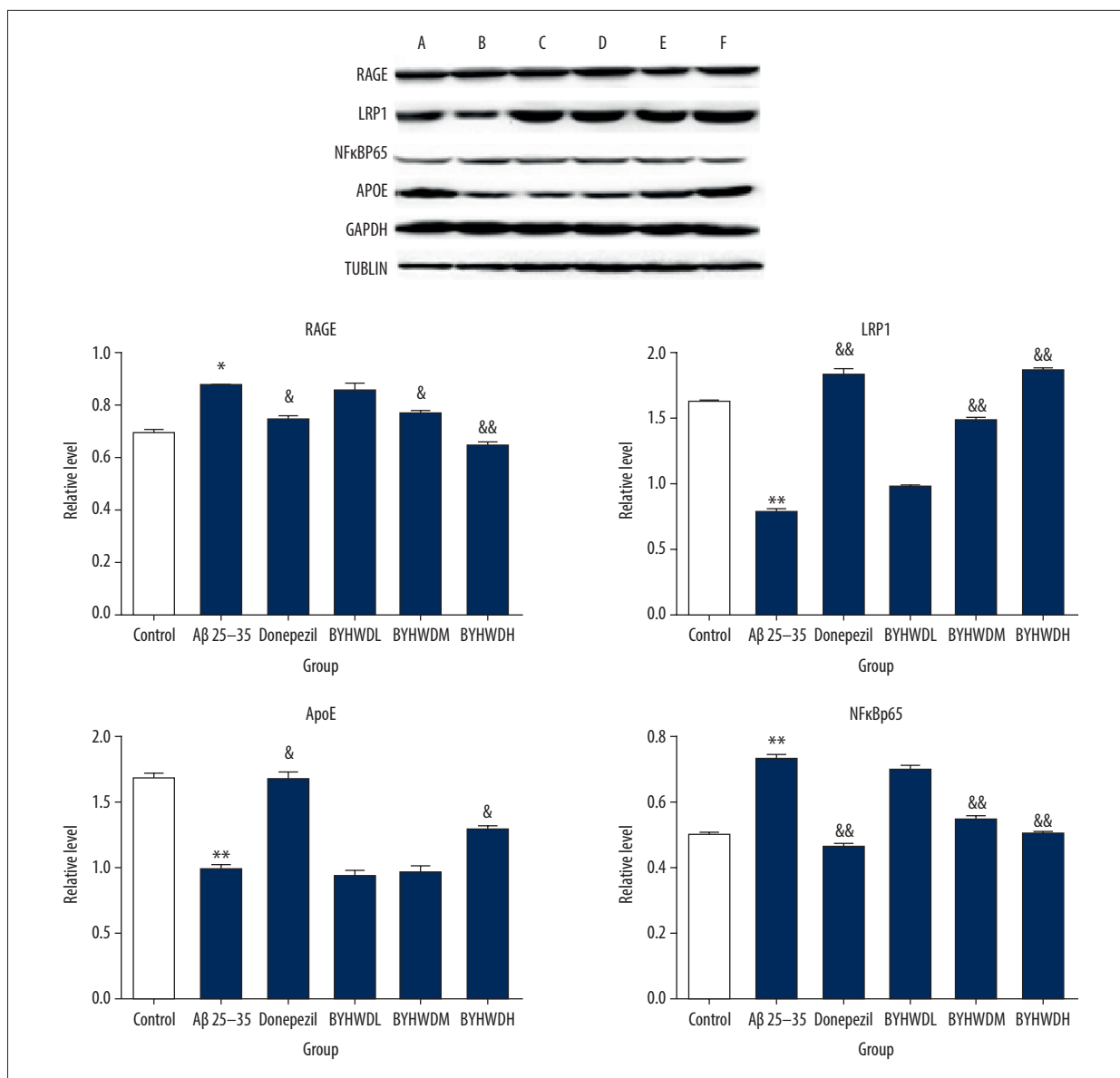
Figure 8. Protein levels of RAGE, LRP1, NFκB-p65, and ApoE in 6 groups. * p<0.05, compared with the control group; & *P*<0.05, compared with the model group. A – control group; B – model group; C – Donepezil group; D – BYHWDL group; E – BYHWDM group; F – BYHWDH group.

the expression levels of IL-1β, IL-6, and TNF-α were significantly lower than in the Model group (P<0.001). There was no significant difference in expression of IL-1β, IL-6, and TNF-α between the BYHWDM and Donepezil groups. Those findings indicate that the expression levels of IL-1β, IL-6, and TNF-α in BEMCs induced by Aβ were decreased by BYHWD (Figure 7).

Western blotting

Compared to the Control group, the protein expressions of RAGE and NF-κBp65 were significantly increased (*P*<0.01), while the expressions of LRP1 and Apo E was significantly

decreased (*P*<0.01) in the Model group. The results indicated that the model induced by Aβ$_{25-35}$ was similar to the pathological changes of AD, and thus the model establishment was considered successful. The protein expressions of RAGE and NF-κBp65 in BYHWD groups with different doses were significantly decreased in a dose-dependent manner compared to the Model group, especially the BYHWDH group (*P*<0.05). There was no significant difference in expression of Apo E between the BYHWDL and BYHWDM groups, but the BYHWDH group had a significant difference. These findings suggested that the therapeutic effect of BYHWD on AD is mediated by the RAGE/LRP1 transfer system and NF-κBp65 pathway (Figure 8).
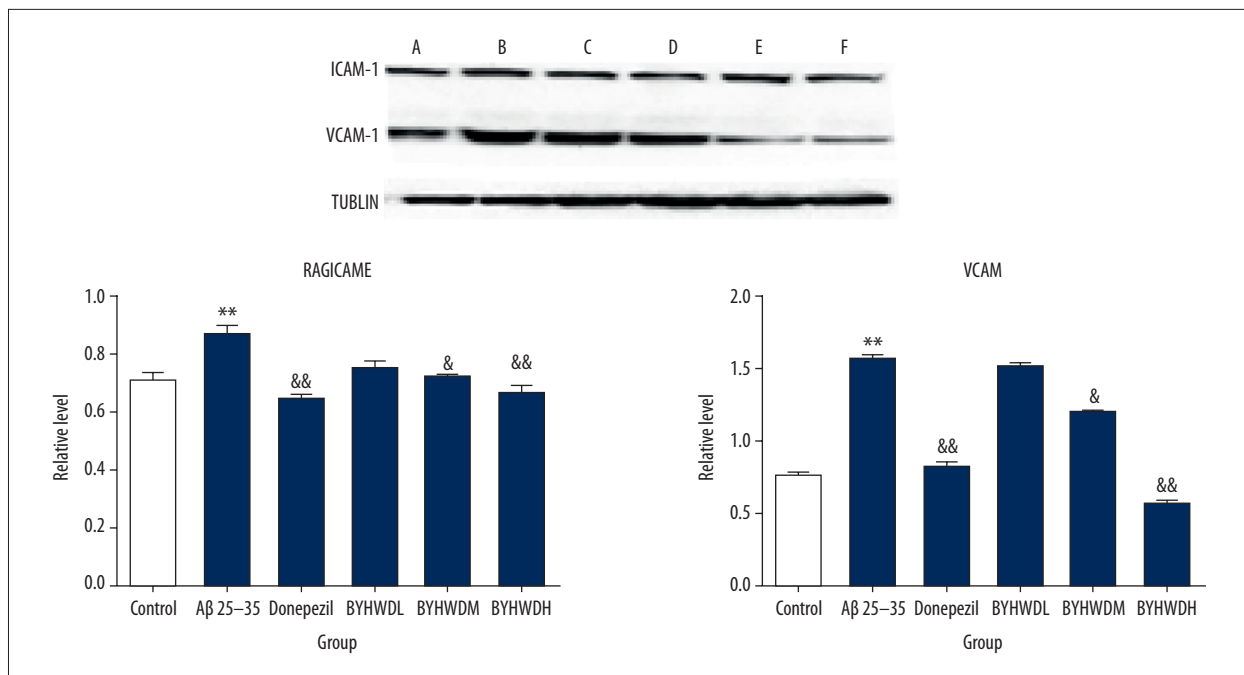
Figure 9. Protein levels of ICAM-1 and VCAM-1 in 6 groups. * $P<0.05$, ** $P<0.01$ compared with the control group; & $P<0.05$, && $P<0.01$, compared with the model group. A – control group; B – model group; C – Donepezil group; D – BYHWDL group; E – BYHWDM group; F – BYHWDH group.

In the Model group, $A\beta_{25-35}$ stimulated vascular endothelial cells to produce inflammation and increased the protein expressions of ICAM, NF-κBp65, and VCAM-1 ($P<0.01$). The results indicated that therapy with $A\beta_{25-35}$ for 24 h caused inflammatory lesions of brain microvascular endothelial cells, thus affecting the permeability of endothelial cells. The protein expressions of ICAM-1 and VCAM-1 in BYHWD groups with different doses were more significantly decreased compared to the Model group, in a dose- dependent manner. Furthermore, BYHWDM and BYHWDH had the most obvious effect on the decrease of ICAM-1 and VCAM-1 ($P<0.05$). These findings suggested that the therapeutic effect of BYHWD on AD was mediated by inhibiting NF-κBp65 pathway, which was achieved by affecting ICAM-1 and VCAM-1 proteins (Figure 9).

Discussion

AD, a profound neurodegenerative disease in elderly people, affects cognition, behavior, and function [21]. It is widely acknowledged that deposition of Aβ is one of the main typical pathological characteristics of AD [22]. Prior studies have demonstrated that BYHWD promotes neurological rehabilitation after cerebral ischemic injury by improving synaptic plasticity [23–25]. In addition, the involvement of RAGE in pathophysiological processes has been proven in some neurodegenerative diseases [26]. Oxidative stress is increased after binding ligands to RAGE. In addition, overexpression of RAGE can lead to a harmful

cycle that perpetuates oxidative stress and contributes to neuroinflammation by nuclear factor-κB (NF-κB) upregulation [26]. Therefore, in the present study we investigated the effect of BYHWD on BMECs induced by $A\beta_{25-35}$ and explored the relationship between RAGE/LRP1 and NF-κBp65 in AD.

Our research demonstrated that BYHWD improves the damage of BMECs induced by $A\beta_{25-35}$, and it has a certain protective effect on BMECs. The apoptosis rate of BMECs in the Model group was significantly increased compared to the Control group, while the BYHWD high-dose and medium-dose groups had lower apoptosis rates of BMECs in different degrees. In addition, the result of electron microscopy showed obvious decrease of apoptotic bodies in the BYHWDH and BYHWDM groups, and these findings were consistent with morphological experimental results of BMECs. Studies showed that extracellular deposition of Aβ may induce neuronal death, which is the major cause of AD [27,28]. The chronic inflammatory cascade of brain tissue caused by Aβ-mediated neuronal injury is an important part of the pathological process of AD [29]. Thus, we used ELISA to assess the role of BYHWD in the expression of inflammatory factors and $A\beta_{25-35}$ protein in BMECs. The expression of inflammatory cytokines IL-1β, IL-6, TNF-α, and $A\beta_{25-35}$ in the Model group was significantly higher than in the Control group, indicating that successful modeling was achieved. Furthermore, different concentrations of BYHWD decreased the expression of inflammatory cytokines IL-1β, IL-6, TNF-α, and $A\beta_{25-35}$, indicating that BYHWD regulates the

immune inflammatory cascade caused by excessive deposition of Aβ. BYHWD effectively reduces neuronal injury induced by Aβ toxicity in brain tissue, and can prevent and treat AD.

In this study, the effect of BYHWD on RAGE/LRP1 transporter in BMECs and its protective effect on endothelial cells were investigated. The results showed that BYHWD decreased the expression of the inward transporter RAGE and increased the expression of the outward transporter LRP1 and the key ligand ApoE. Downregulation of the inward transporter RAGE reduces its ability to enter brain tissue, thereby reducing the accumulation of free Aβ in the brain tissue. Upregulation of the outward transporter LRP1 and the key ligand ApoE accelerates the transport of Aβ across BBB, thereby effectively reducing the formation of Aβ and senile plaques (SP) in brain tissue [22]. This study demonstrated that the interaction between Aβ and RAGE can activate NF-κB, which mediates vascular endothelial activation and increases the expression of inflammatory cytokines TNF-6 and IL-6 and adhesion molecules ICAM-1 and VCAM-1 and endothelin-1 (ET-1) to promote inflammatory

response and the development of AD. Thus, both RAGE expression and adhesion factors (ICAM-1 and VCAM) expression are closely associated with activation of NF-κB.

Conclusions

Our research demonstrated that 20 nmol/L $A\beta_{25-35}$ leads to protein expression disorder of RAGE/LRP1 and overexpression of inflammatory factors such as ICAM-1 and VCAM-1. BYHWD improves morphological changes in BMECs induced by Aβ. BYHWD regulates Aβ metabolism via the RAGE/LRP1 pathway and inhibits vascular endothelial inflammation induced by ICAM-1 and VCAM-1 via the NF-κBP65 pathway. These results provide reliable experimental evidence of the effects of BYHWD treatment on AD.

Conflict of interest

None.

References:

1. Guo YX, He LY, Zhang M et al: 1,25-Dihydroxyvitamin D3 regulates expression of LRP1 and RAGE *in vitro* and *in vivo*, enhancing Abeta1-40 brain-to-blood efflux and peripheral uptake transport. Neuroscience, 2016; 322: 28–38

2. Chen YG: Research progress in the pathogenesis of Alzheimer's disease. Chin Med J (Engl), 2018; 131: 1618–24

3. Zhou L, Huang Y, Xie H, Mei X: Buyang Huanwu Tang improves denervation-dependent muscle atrophy by increasing ANGPTL4, and increases NF-κB and MURF1 levels. Mol Med Rep, 2018; 17: 3674–80

4. Anand A, Patience AA, Sharma N, Khurana N: The present and future of pharmacotherapy of Alzheimer's disease: A comprehensive review. Eur J Pharmacol, 2017; 815: 364–75

5. Sharif NA: iDrugs and iDevices Discovery Research: Preclinical assays, techniques, and animal model studies for ocular hypotensives and neuroprotectants. J Ocul Pharmacol Ther, 2018; 34: 7–39

6. Cai Z, Liu N, Wang C et al: Role of RAGE in Alzheimer's disease. Cell Mol Neurobiol, 2016; 36: 483–95

7. Wan W, Chen H, Li Y: The potential mechanisms of Abeta-receptor for advanced glycation end-products interaction disrupting tight junctions of the blood-brain barrier in Alzheimer's disease. Int J Neurosci, 2014; 124: 75–81

8. Schwenger V, Morath C, Salava A et al: Damage to the peritoneal membrane by glucose degradation products is mediated by the receptor for advanced glycation end-products. J Am Soc Nephrol, 2006; 17: 199–207

9. Wang CY, Xie JW, Xu Y et al: Trientine reduces BACE1 activity and mitigates amyloidosis via the AGE/RAGE/NF-kappaB pathway in a transgenic mouse model of Alzheimer's disease. Antioxid Redox Signal, 2013; 19: 2024–39

10. Kvartsberg H, Duits FH, Ingelsson M et al: Cerebrospinal fluid levels of the synaptic protein neurogranin correlates with cognitive decline in prodromal Alzheimer's disease. Alzheimers Dement, 2015; 11: 1180–90

11. Agrawal S, Abud EM, Snigdha S, Agrawal A: IgM response against amyloid-beta in aging: A potential peripheral protective mechanism. Alzheimers Res Ther, 2018; 10(1): 81

12. Flemmig J, Zamocky M, Alia A: Amyloid beta and free heme: Bloody new insights into the pathogenesis of Alzheimer's disease. Neural Regen Res, 2018; 13: 1170–74

13. Fulop T, Witkowski JM, Bourgade K et al: Can an infection hypothesis explain the beta amyloid hypothesis of Alzheimer's disease? Front Aging Neurosci, 2018; 10: 224

14. Mantle JL, Lee KH: A differentiating neural stem cell-derived astrocytic population mitigates the inflammatory effects of TNF-alpha and IL-6 in an iPSC-based blood-brain barrier model. Neurobiol Dis, 2018; 119: 113–20

15. Oh S, Son M, Choi J et al: sRAGE prolonged stem cell survival and suppressed RAGE-related inflammatory cell and T lymphocyte accumulations in an Alzheimer's disease model. Biochem Biophys Res Commun, 2018; 495: 807–13

16. Cui HJ, Yang AL, Zhou HJ et al: Buyang huanwu decoction promotes angiogenesis via vascular endothelial growth factor receptor-2 activation through the PI3K/Akt pathway in a mouse model of intracerebral hemorrhage. BMC Complement Altern Med, 2015; 15: 91

17. Hung IL, Hung YC, Wang LY et al: Chinese herbal products for ischemic stroke. Am J Chin Med, 2015; 43: 1365–79

18. Liu X, Min Y, Gu W et al: Buyanghuanwu Tang therapy for neonatal rats with hypoxic ischemic encephalopathy. Int J Clin Exp Med, 2015; 8: 18448–54

19. Zhou L, Huang Y, Xie H, Mei X: Buyang Huanwu Tang improves denervation-dependent muscle atrophy by increasing ANGPTL4, and increases NF-kappaB and MURF1 levels. Mol Med Rep, 2018; 17: 3674–80

20. Wen XD, Liu EH, Yang J et al: Identification of metabolites of Buyang Huanwu decoction in rat urine using liquid chromatography – quadrupole time-of-flight mass spectrometry. J Pharm Biomed Anal, 2012; 67–68: 114–22

21. Hu Q, Yu B, Chen Q et al: Effect of Linguizhugan decoction on neuroinflammation and expression disorder of the amyloid β-related transporter RAGE and LRP-1 in a rat model of Alzheimer's disease. Mol Med Rep, 2018; 17(1): 827–34

22. Li XH, Deng YY, Li F et al: Neuroprotective effects of sodium hydrosulfide against beta-amyloid-induced neurotoxicity. Int J Mol Med, 2016; 38: 1152–60

23. Shen J, Zhu Y, Yu H et al: Buyang Huanwu decoction increases angiopoietin-1 expression and promotes angiogenesis and functional outcome after focal cerebral ischemia. J Zhejiang Univ Sci B, 2014; 15: 272–80

24. Mu Q, Liu P, Hu X et al: Neuroprotective effects of Buyang Huanwu decoction on cerebral ischemia-induced neuronal damage. Neural Regen Res, 2014; 9: 1621–27

25. Pan R, Cai J, Zhan L et al: Buyang Huanwu decoction facilitates neurorehabilitation through an improvement of synaptic plasticity in cerebral ischemic rats. BMC Complement Altern Med, 2017; 17: 173

26. Tóbon-Velasco JC, Elvis C, Torres-Ramos MA: Receptor for AGEs (RAGE) as mediator of NF-κB pathway activation in neuroinflammation and oxidative stress. CNS Neurol Disord Drug Targets, 2014; 13: 1615–26

27. Mallat Z, Gojova A, Sauzeau V et al: Rho-associated protein kinase contributes to early atherosclerotic lesion formation in mice. Circ Res, 2003; 93: 884–88

28. Rego A, Viana SD, Ribeiro CA et al: Monophosphoryl lipid-A: A promising tool for Alzheimer's disease toll. J Alzheimers Dis, 2016; 52: 1189–202

29. Jiang T, Tan L, Gao Q et aL: Plasma angiotensin-(1-7) is a potential biomarker for Alzheimer's disease. Curr Neurovasc Res, 2016; 13: 96–99